Excitatory and inhibitory D-serine binding to the NMDA receptor

Remy A. Yovanno[1], Tsung Han Chou[2], Sarah J. Brantley[3], Hiro Furukawa[2*], and Albert Y. Lau[1*]

Affiliations:

[1]Department of Biophysics and Biophysical Chemistry, Johns Hopkins University School of Medicine, 725 N. Wolfe Street, WBSB 706, Baltimore, MD 21205, USA.

[2] W.M. Keck Structural Biology Laboratory, Cold Spring Harbor Laboratory, Cold Spring Harbor, NY 11724, USA.

[3]Department of Biology, Johns Hopkins University, 3400 N. Charles Street, Baltimore, MD 21218, USA

[*] To whom correspondence should be addressed:

alau@jhmi.edu (A.Y.L.)

furukawa@cshl.edu (H.F.)

ABSTRACT

N-methyl-D-aspartate receptors (NMDARs) uniquely require binding of two different neurotransmitter agonists for synaptic transmission. D-serine and glycine bind to one subunit, GluN1, while glutamate binds to the other, GluN2. These agonists bind to the receptor's bi-lobed ligand-binding domains (LBDs), which close around the agonist during receptor activation. To better understand the unexplored mechanisms by which D-serine contributes to receptor activation, we performed multi-microsecond molecular dynamics simulations of the GluN1/GluN2A LBD dimer with free D-serine and glutamate agonists. Surprisingly, we observed D-serine binding to both GluN1 and GluN2A LBDs, suggesting that D-serine competes with glutamate for binding to GluN2A. This mechanism is confirmed by our electrophysiology experiments, which show that D-serine is indeed inhibitory at high concentrations. Although free energy calculations indicate that D-serine stabilizes the closed GluN2A LBD, its inhibitory behavior suggests that it either does not remain bound long enough or does not generate sufficient force for ion channel gating. We developed a workflow using pathway similarity analysis to identify groups of residues working together to promote binding. These conformation-dependent pathways were not significantly impacted by the presence of N-linked glycans, which act primarily by interacting with the LBD bottom lobe to stabilize the closed LBD.

INTRODUCTION

The N-methyl-D-aspartate receptor (NMDAR) is an ionotropic glutamate receptor (iGluR) that uniquely requires the binding of a co-agonist in addition to its primary

44 agonist for activation. This heterotetrameric ion channel comprises at least two different
45 subunits, GluN1 (isoforms 1-4a and 1-4b) and GluN2 (subtypes A-D), assembled as a
46 dimer of GluN1/GluN2 heterodimers. The GluN2 subunit binds the neurotransmitter
47 glutamate, while the GluN1 subunit can either bind the co-agonists glycine or D-serine.
48 Traditionally, glycine had been considered the dominant GluN1 agonist [1–3], but more
49 recent work has suggested that D-serine may in fact be the dominant co-agonist for
50 synaptic NMDARs in the brain [4]. D-serine is synthesized by the enzyme serine
51 racemase expressed in astroglia [5] and neurons [6] [7] and is released into the
52 postsynapse by the Asc-1 transporter [8] [9]. D-serine binding to these synaptic
53 NMDARs is responsible for inducing long-term potentiation (LTP), which is critical for
54 memory functions [10]. In addition, recent clinical efforts have indicated that D-serine
55 could be a promising therapeutic for the treatment of neuropsychiatric disorders
56 [11][12], most notably schizophrenia [13] and post-traumatic stress disorder (PTSD)
57 [14]. Unlike the more well-studied agonists glutamate and glycine, the role of D-serine is
58 less defined, causing it to be known as the “shape-shifting” agonist [9] that can adopt
59 different roles in neurotransmission.
60 Each NMDAR subunit consists of an amino-terminal domain (ATD), a ligand-
61 binding domain (LBD; also called an agonist-binding domain, ABD), a transmembrane
62 domain (TMD), and a disordered cytoplasmic C-terminal domain [15]. The LBDs adopt a
63 bi-lobed clamshell architecture that close upon agonist binding. Previous computational
64 studies of NMDAR LBDs have indicated that glycine binding to the GluN1 LBD and
65 glutamate binding to the GluN2A LBD drives the conformational equilibrium toward the
66 closed LBD [16]. While crystallographic studies have determined the binding pose of D-

67 serine bound to the closed GluN1 LBD [17], the molecular mechanisms by which D-
68 serine finds its way into and stabilizes NMDAR LBDs is not well understood.
69 Previous simulation studies have revealed the mechanisms by which glycine and
70 glutamate diffuse into the LBD binding site [18]. Specifically, they found that glycine
71 binds to the GluN1 subunit by freely diffusing into the binding pocket, where it is trapped
72 by energetically favorable interactions with key binding site residues. Glutamate, on the
73 other hand, was found to contact residues along the protein surface that helped guide
74 itself into its binding pocket, positioning it to interact stably with residues in the binding
75 site. These two binding mechanisms were referred to as “unguided" and "guided"
76 diffusion, respectively [19]. This paradigm established the two extremes by which
77 ligands enter their receptor sites: one in which stable ligand binding only depends upon
78 the identity of the binding site residues and another that also heavily relies on residues
79 outside the binding site to guide the ligand toward its bound pose.
80 Performing multi-microsecond molecular dynamics simulations of the
81 glycosylated GluN1/GluN2A LBD dimer, we identified binding mechanisms and residues
82 critical for promoting D-serine binding and stabilization by developing a new binding
83 pathway clustering workflow. Surprisingly, we observed D-serine binding to both GluN1
84 and GluN2A LBDs. We determined that D-serine binding to GluN2A partially stabilizes
85 the active LBD conformation. Inspired by these simulation results, we determined that
86 D-serine competes with glutamate for binding to GluN2A via a competitive inhibition
87 mechanism using electrophysiology measurements, where D-serine was found to be
88 inhibitory at high concentrations. Since NMDAR LBDs are glycosylated under
89 physiological conditions [20], including N-linked glycans in our simulations revealed that

90 glycans primarily regulate the binding process by stabilizing the active LBD. In total, we
91 investigated the molecular components contributing to D-serine binding and
92 stabilization, highlighting the complex components driving neurotransmission.
93

94 **RESULTS**

95 ***D-serine binding pathways for GluN2A and GluN1 LBDs***

96 In simulating the GluN1/GluN2A LBD dimer, which is a physiological NMDAR
97 unit, we intended to focus our attention on the mechanisms by which D-serine binds to
98 the GluN1 LBD, the subunit to which D-serine is a potent agonist. However, in our
99 simulations, we also observed a significant number of D-serine binding events involving
100 the GluN2A LBD, an unexpected finding. These binding events are primarily made up of
101 guided-diffusion pathways in which D-serine contacts key residues on the LBD surface
102 to help guide it into the binding cleft. In our aggregate ~51 μs of sampling of the
103 glycosylated GluN1/GluN2A LBD dimer, we identified 99 guided-diffusion pathways for
104 GluN2A and 104 (plus 23 free diffusion events) for GluN1. Due to the stochastic nature
105 of these pathways, we needed to develop a reliable way to identify key features of
106 predominant binding pathways. To address this, we applied pathway similarity analysis
107 (PSA) [21] to quantify the spatial and geometric similarity between pairs of paths **(Fig.
108 1A)**. Here, we extend this application to ligand binding pathways by monitoring the
109 change in ligand C_α position throughout each path. This allowed us to cluster paths
110 traversing similar regions of the LBD surface. To aid in describing the different faces of
111 the LBD, we use an order parameter (ξ_1, ξ_2) defined in previous work [16] to describe
112 whether D-serine primarily contacts residues on the ξ_1 or ξ_2 face of the LBD **(Fig. 1B,**

113 **2A)**. For GluN2A, cluster analysis revealed four distinct regions of D-serine occupancy.
114 The clusters correspond to the following methods of binding: 1. D-serine approaches
115 the binding pocket from the ξ_2 face; 2. D-serine contacts the D1 residues on the ξ_1 face;
116 3. D-serine zigzags between D1 and D2 lobes on the ξ_1 face; 4. D-serine primarily
117 contacts residues on the D2 lobe of the ξ_1 face **(Fig. 1C-F)**. Similarly, for GluN1, cluster
118 analysis revealed four distinct clusters corresponding to similar pathways of binding: 1.
119 D-serine contacts the ξ_2 face; 2. D-serine zigzags between D1 and D2 lobes on the ξ_1
120 face; 3. D-serine contacts residues on the N-terminal (top) end of D1 of the ξ_1 face; 4.
121 D-serine contacts residues of D1 loop 2 that protrudes from the LBD into solution. We
122 then analyzed the resulting clusters to identify key residues that guide D-serine into the
123 binding site **(Fig. 2B-E)**. Interestingly, we observed that GluN1 pathways involve fewer
124 interactions between D-serine and D2 residues; most notably, there were fewer
125 contacts with Helix F (Helix E for GluN2A) compared to GluN2A pathways.
126 To quantify the extent to which these clusters involve similar residue contacts, we
127 used a pairwise similarity metric called the overlap coefficient (i.e., Szymkiewicz–
128 Simpson coefficient) that describes agreement between sets of residues [22]. Doing so
129 provides a way to determine whether these spatial clusters are mostly made up of
130 random contacts, or whether groups of residues tend to act together to promote binding,
131 allowing us to quantify the extent to which agonist diffusion is "guided" by contacts along
132 the LBD. For GluN2A, we computed the overlap coefficient for all path pairs in each
133 cluster for comparison with the global mean (global $\langle OC \rangle$ = 0.557) **(Fig. S1A)**. We found
134 that pathway pairs in three of the four clusters yielded an overlap coefficient greater
135 than the mean of all pairs of paths from all clusters, indicating that pathways in each

136 cluster are made up of specific residue contacts **(Fig. S1C)**. In contrast, for GluN1, a
137 significant cluster (26 paths) involving interactions with residues on the ξ_2 face of the
138 LBD has a cluster mean OC much less than the global mean (global $\langle OC \rangle$ = 0.671),
139 indicating that this cluster primarily comprises random contacts **(Fig. 1B, S1B,D)**. This
140 suggests that D-serine binding to GluN1 may be more diffusion-driven and less guided
141 than to GluN2A. Therefore, we propose that agonist binding mechanisms exist on a
142 spectrum ranging from unguided to guided diffusion. The difference in the specificity of
143 D-serine contacts along binding pathways for GluN2A and GluN1 suggests that the
144 extent to which agonists rely on pathways of guiding residues depends on LBD
145 architecture and not solely upon the identity of the agonist.

146 Mapping important pathway residues onto the intact GluN1/GluN2A NMDAR
147 (PDB ID: 6MMM [23]) further enriches our understanding of binding pathways by
148 allowing us to determine whether residues in particular pathways are accessible for
149 binding or obscured by other receptor domains and subunits. For GluN2A, access to
150 residues on the extreme of the ξ_2 face is slightly restricted by the presence of the GluN1
151 subunit of the adjacent LBD dimer **(Fig. S2A)**. However, this interface does not seem to
152 be near the specific residues identified as critical for binding. Even more restricted is
153 access to residues on the ξ_1 face of GluN1, which are obscured by GluN2A of the
154 adjacent LBD dimer, including residues identified as critical for binding pathways **(Fig.
155 S2B)**. This might bias the pathways observed for the intact receptor by forcing the
156 agonist to favor residues on the ξ_2 face of the LBD. Since our overlap coefficient
157 analysis of the cluster that corresponds to the ξ_2 face of GluN1 identified more non-
158 specific interactions, it is possible that the D-serine mechanism would be biased to favor

159 unguided diffusion. It is also possible that access to residues near the N-terminal end of
160 D1 would be restricted by the R2 lobe of its own ATD.

161 We next investigated whether a specific LBD conformational state was favored
162 for successful D-serine binding pathways. We computed our (ξ_1, ξ_2) order parameter to
163 quantify the degree of closure of the LBDs for all trajectory frames identified as part of
164 binding (and unbinding) pathways and found that (ξ_1, ξ_2) = (16,14) for GluN2A **(Fig.**
165 **S3A)** and (ξ_1, ξ_2) = (11,13) for GluN1 **(Fig. S3B)**. These values correspond to a partially
166 open LBD. The LBD needs to be open enough for the ligand to diffuse into the pocket
167 but closed enough to form some stabilizing interactions with the ligand. However, we
168 notice that the ξ_1 is smaller for GluN1, indicating that agonist binding can occur at
169 slightly more closed LBD conformations. GluN1 pathways where (ξ_1, ξ_2) = (11,13) are
170 mostly in the cluster defined by D-serine interactions with Loop 2, highlighting the role of
171 Loop 2 residues in D-serine binding to GluN1. Overall, these results suggest that the
172 degree of LBD closure does influence the likelihood of successful binding.

173

174 ***Effects of D-serine binding on the LBD conformational free energy landscapes***

175 Since we did not expect to see D-serine binding to the GluN2A LBD, we needed
176 to determine whether these GluN2A D-serine binding events are able to modulate the
177 GluN2A LBD conformation. Since full LBD closure occurs on multi-microsecond to
178 millisecond timescales [24][25][26], direct observation of such a conformational change
179 was not fully captured from our equilibrium binding trajectories. Instead, to ensure we
180 are sampling the full range of LBD conformations, we performed umbrella sampling free
181 energy molecular dynamics simulations to obtain the conformational free energy

182 landscape of GluN2A bound to D-serine **(Fig. 3A)**. We used the order parameter (ξ_1, ξ_2)
183 [16] that captures the opening and closing motion of the LBDs observed in crystal
184 structures of these domains. Since no crystal structure exists for D-serine bound to
185 GluN2A, we identified residues critical for stabilizing the agonist in the closed state by
186 analyzing contacts in lowest-energy (≤1 kcal mol^{-1}) conformers **(Fig. S4A)**. For
187 reference, we compared the resulting energy landscape to those previously computed
188 for the apo- and glutamate-bound GluN2A monomers **(Fig. 3C,D)** [16]. We see that, like
189 glutamate, D-serine stabilizes the closed LBD conformation. The D-serine energy
190 landscape has a global minimum corresponding to (ξ_1, ξ_2) values of (11, 11.5 Å) and a
191 metastable minimum corresponding to (ξ_1, ξ_2) values of (15.5, 11.5 Å). The presence of
192 a metastable agonist-bound LBD partially open intermediate suggests that D-serine
193 may not stabilize the closed conformation to the same extent as glutamate and
194 generate sufficient force to control channel gating. We then compared different
195 conformers corresponding to these two states to determine residues critical for agonist
196 stabilization. The primary difference between the residue contacts in conformers of the
197 two states is the prevalence of interactions with Thr-690 **(Fig. S4B)**, which only contacts
198 D-serine in the more closed state centered at (ξ_1, ξ_2) = (11, 11.5 Å). This is supported by
199 our binding simulations; although we do not fully sample LBD closure, trajectory frames
200 with low (ξ_1, ξ_2) values involve contacts with Thr-690. This suggests that Thr-690 is
201 critically involved in promoting full GluN2A LBD closure upon agonist binding.
202 Experimental binding studies have indicated that D-serine may be a more potent
203 GluN1 agonist than glycine [27]. To better understand the molecular mechanism
204 responsible for this difference in agonist potency, we computed the conformational free

205 energy for the D-serine-bound GluN1 LBD **(Fig. 3F)**. Compared with the previously
206 computed glycine-bound and apo LBDs **(Fig. 3G,H)** [16], the presence of D-serine in
207 the binding cleft results in a greater population of conformers in the closed conformation
208 and fewer conformers adopting a more open conformation. Similar to GluN2A Thr-690,
209 GluN1 Asp-732 and (to a lesser extent) Ser-688 help stabilize D-serine in the closed
210 LBD conformation by interacting with the D-serine hydroxyl. For this reason, we propose
211 that D-serine's high potency is due, at least in part, to its ability to more strongly
212 stabilize a closed LBD through additional interactions with the D2 lobe.
213
214 ***D-serine and glutamate compete for binding to the GluN2A LBD***
215 Since our simulations revealed that D-serine can enter the GluN2A LBD binding
216 pocket and partially stabilize the active conformation, we hypothesized that D-serine
217 might compete with glutamate for binding to GluN2A. In fact, we observed D-serine
218 binding to GluN2A, even in the presence of glutamate, although glutamate bound more
219 frequently than D-serine and with longer residence times in the binding site **(Datasets**
220 **S2, S3)**. Since increasing the D-serine concentration would increase the frequency of D-
221 serine binding to GluN2A, it is possible that D-serine could function as an inhibitor
222 (competitive antagonist) at high concentrations. If true, this behavior may factor into
223 therapeutic strategies focused on increasing D-serine concentration in the synapse by
224 establishing an upper dosage limit after which a D-serine increase is no longer
225 potentiating.
226 To probe this behavior experimentally, we measured GluN1-2A NMDAR currents
227 using two-electrode voltage clamp (TEVC) electrophysiology. We observed that at high

228 (~1 mM) D-serine concentrations, NMDAR activity was inhibited **(Fig. 4A)**. The inhibition
229 was dependent on glutamate concentrations, implying that the inhibitory effect of D-
230 serine may be competitive **(Fig. 4B)**. Furthermore, dose-response curves of glutamate
231 activation were right-shifted in the presence of increasing concentrations of D-serine
232 **(Fig. 4C)**. The calculated slope value of the Schild plot at 1.1 ± 0.1 implied that D-serine
233 and glutamate likely compete against each other **(Fig. 4C)**. Combined with our
234 simulation results, our electrophysiological data supports the hypothesis that D-serine at
235 high concentrations can bind to the GluN2A subunit and compete against glutamate.
236 Since a similar inhibitory effect was also observed at high glycine concentrations
237 by TEVC electrophysiology **(Fig. 4A)**, we repeated our umbrella sampling simulations
238 with glycine bound to the GluN2A LBD. We see that glycine also favors the closed LBD
239 **(Fig. 3B)**. The lowest-energy conformers of GluN2A with glycine are fastened shut by
240 contacts between the N-terminal amine of glycine and Tyr-730. Although glutamate still
241 stabilizes the closed GluN2A LBD to the greatest extent, comparable thermodynamics
242 between different agonists suggests that kinetics of agonist binding and unbinding is a
243 critical driver of agonist-induced activation. The GluN2A LBD likely never closes around
244 glycine because glycine does not remain bound long enough to induce LBD closure.
245 Previous binding studies [18] have indicated that glutamate, the primary GluN2A
246 agonist, similarly relies on LBD surface residues to promote binding. To determine
247 whether D-serine and glutamate binding are guided by similar residue contacts, we
248 computed the overlap coefficient between residues in D-serine and glutamate pathways
249 to be 0.964 for the glycosylated GluN2A LBD, corresponding to a significant overlap in

250 agonist occupancy **(Fig. 5A)**. This high degree of overlap between glutamate and D-
251 serine pathway residues indicates that they bind through similar mechanisms.
252 Despite similar pathway residues, we identified key residues that distinguish
253 glutamate from D-serine binding pathways **(Fig. 5B and Dataset S7)**. Most of the
254 residues important for D-serine binding, but not for glutamate binding, are located on
255 the ξ_2 face of the LBD. Most notably, Glu-413, Tyr-730, Ser-511, and Asp-731 all occur
256 in D-serine binding pathways with a frequency of more than ten times their fractional
257 occurrence in glutamate binding pathways. It is important to note, however, that
258 glutamate does interact with residues on the ξ_2 face, but the specific nature of those
259 contacts differ between the two agonists. In contrast, we found that Lys-487 is
260 contacted with significantly greater frequency in glutamate binding pathways. Due to
261 these residues' close proximity to the binding cleft, it is likely that these residues are
262 responsible for facilitating proper positioning of the agonists in the binding site, based
263 on differences in agonist size and shape.
264 An important feature of glutamate binding to GluN2A is its ability to bind in an
265 inverted pose relative to the crystal structure, which we observed in previous
266 simulations [18] [19]. Since no experimental structure exists for glutamate bound in the
267 inverted pose, we performed umbrella sampling simulations to determine the free
268 energy landscape of the GluN2A LBD with glutamate bound in the inverted pose **(Fig.
269 3E)**. We found that glutamate bound in the inverted pose prevents full LBD closure as
270 predicted in previous work [18]. Specifically, glutamate in the inverted pose stabilizes a
271 conformation centered around (ξ_1, ξ_2) values of (14, 13 Å). Comparing the low-energy
272 conformers of D-serine and inverted glutamate ($\leq$ 1 kcal mol^{-1}) with the glutamate-

273 bound crystal structure, we found that D-serine and glutamate are stabilized by the
274 same residues, although there are fewer interactions between Thr-690 and glutamate in
275 the inverted pose, further supporting the importance of this residue for stabilizing the
276 fully closed LBD.
277
278 ***Kinetic analysis of D-serine binding pathways***
279 We computed the D-serine association rate constant (k_{on}) for GluN2A and GluN1
280 LBDs using a method described [28] and used in previous iGluR work [19] as
281 summarized in the equation below:
282
$$k_{\mathrm{on}} = \frac{N_b}{\sum_i \frac{t_i[L_i]}{s_i}}.$$
283
284 Here, N_b is the number of association events, t_i is the time the agonist spends in bulk
285 solvent, s_i is the number of identical binding sites, and $[L_i]$ is the concentration of free
286 agonist. One advantage of this approach is the ability to combine simulations performed
287 at various concentrations of free agonist $[L_i]$. Here, k_{on} is a bulk property and relies on
288 fully sampling the LBD conformational landscape throughout the simulation. However,
289 our binding simulations fail to adequately sample the agonist-bound, closed LBD state.
290 This affects both the number of observed binding events N_b and the time the agonist
291 spends in bulk solvent (t_i). Since this value is most sensitive to the number of identified
292 binding events N_b, we computed the k_{on} for different N_b values based on the duration of
293 the resulting binding event. This minimizes contributions from extremely short binding
294 events that are unlikely to be functionally relevant. For GluN2A, this results in a D-serine
295 k_{on} with an upper bound of 7.8×10^7 $M^{-1}s^{-1}$ (all events included) and a lower bound of

296 1.6×10^7 $M^{-1}s^{-1}$ (only events with agonist residence times > 100 ns were included). For
297 GluN1, the upper bound for k_{on} is 9.0×10^7 $M^{-1}s^{-1}$ and the lower bound is 7.0×10^6 M^{-}
298 $^{1}s^{-1}$. Based on these values, it is reasonable to expect that D-serine binds to GluN2A
299 and GluN1 at similar rates. For comparison, the association rate constants computed for
300 glutamate binding to GluN2A with this method range from 4.9×10^7 $M^{-1}s^{-1}$ to 1.4×10^8
301 $M^{-1}s^{-1}$. Similar ranges of D-serine binding rate constants for GluN2A and GluN1 support
302 our data indicating a guided-diffusion mechanism. However, this definition of the
303 association rate constant does not capture the molecular details that produce this bulk
304 behavior.

305 For agonist binding mechanisms dominated by guided diffusion, we can monitor
306 how much time the agonist spends (1) in bulk solvent, (2) associated with the LBDs,
307 and (3) docked in the binding cleft (interacting with the conserved arginines Arg-523 for
308 GluN1 or Arg-518 for GluN2A). Transitions between these states can be represented by
309 the following three-step process:

310

311 $$P + L \rightleftharpoons PL_{\mathrm{assoc}} \rightleftharpoons PL_{\mathrm{docked}} .$$

312

313 Here, the PL_{assoc} state either results in successful binding (represented by pathways) or
314 nonspecific interactions resulting in dissociation. From the clusters of residues that we
315 identified in our pathway similarity analysis, we determined to what extent a particular
316 residue is critical for guiding the agonist into the binding site using a conditional
317 probability-based framework **(Datasets S9, S10)**. For GluN2A, given that a binding
318 event results in successful agonist docking, residues Asp-515, Glu-517, Arg-692, Asn-

319 687, Lys-487, Lys-484, and Ser-689, Lys-488, Ser-511, and Glu-413 are contacted
320 most frequently across all datasets. Given successful D-serine binding, contacts with
321 GluN1 residues Lys-496, Lys-495, Trp-498, Arg-489, and Glu-497 occur in the greatest
322 number of pathways. Slightly less agreement in crucial GluN1 binding residues across
323 datasets further supports a more diffusive/random binding mechanism for D-serine
324 binding to GluN1.
325
326 ***Role of N-linked glycans in D-serine binding pathways***
327 In addition to identifying residues that are responsible for agonist specificity in
328 binding pathways, we also explored the effect of the N-linked $Man_5GlcNAc_2$ (Man5)
329 glycans **(Fig. S6A)** on the residues involved in agonist binding pathways. Previous
330 electrophysiological studies have indicated that glycans function as LBD potentiators
331 [29]. In our simulations, we observed that near-pocket glycans appear to "reach" into the
332 binding pocket. This reaching behavior was observed in previous simulations of the
333 glycosylated NMDAR LBDs in which the glycan forms a "cage" around the binding
334 pocket by forming interactions with the LBD D2 lobe and is believed to be associated
335 with NMDAR potentiation by glycans [29]. For GluN2A, there are two glycans that are
336 near the binding pocket: N443-Man5 and N444-Man5, both of which can interact with
337 the LBD D2 lobe **(Fig. 6A)**. For GluN1, there is a single glycan N491-Man5 that adopts
338 this caged conformation **(Fig. 6B)**. To quantify this behavior in our simulations, we
339 developed a general order parameter to describe the relationship between the glycan
340 and the LBD D2 lobe that measured the minimum distance between any glycan heavy
341 atom and any residue on the LBD D2 lobe. From this order parameter, we computed

342 glycan PMFs along the glycan-D2 order parameter for each near-pocket glycan **(Fig.**
343 **6C-E)**.

344 We compared our glycosylated trajectories with an additional 30 μs of simulations
345 of the non-glycosylated GluN1/GluN2A LBD dimer to identify ways in which the
346 presence of glycans influence binding pathways. Our data indicate that residues on the
347 ξ_2 face are contacted more frequently in non-glycosylated simulations, although these
348 residues are important for D-serine binding with and without glycans **(Dataset S11)**.
349 GluN2A residues Asp-515 and Glu-517, are contacted more frequently in glycosylated
350 systems. The frequency with which D-serine interacts with GluN1 residue Arg-489 in
351 pathways is greater for glycosylated pathways than those without glycans. On average,
352 glycan-mediated D-serine interactions result in slightly longer pathways, suggesting that
353 the presence of glycans slows down the binding process, setting up small kinetic
354 "traps".

355 When we analyzed glycan behavior in our binding pathways, we found that very
356 few D-serine binding pathways (27% for both GluN2A and GluN1) involve contacts with
357 glycans. While glycan-agonist interactions make up a small percentage of time spent in
358 binding pathways (10% for GluN2A and GluN1 D-serine pathways), patterns in glycan
359 interactions with the agonist as it binds suggest that glycans contribute to binding
360 pathways in a consistent way. The most common glycan-mediated D-serine-LBD
361 interactions for GluN2A involve an interaction network formed by N443-Man5 with Glu-
362 412, Lys-438 **(Fig. S6B)**, Lys-738, Glu-413 **(Fig. S6C)**, Tyr-730, and Ser-511 **(Fig.**
363 **S6D)**, as D-serine moves into the binding pocket. Another contact network formed by
364 N444-Man5 with Lys-487, Asn-687 **(Fig. S6E)**, Arg-692, Arg-695, **(Fig. S6F)**, and Glu-

365 413 (alongside the N443-Man5 glycan). For GluN1, the N491-Man5 glycan interacts
366 with D-serine, trapping it in a network of interactions dominated by Arg-489 **(Fig. S6G)**.
367 When formed, this contact network functions as a kinetic trap that results in longer
368 binding pathways. Additionally, the N440-Man5 glycan also contacts D-serine as it
369 interacts with Arg-489 and Glu-497 **(Fig S6H)**. It is interesting to note that, unlike the
370 glycan-mediated contacts identified for GluN2A, glycan-mediated agonist contacts for
371 GluN1 do not involve D2 lobe residues. These glycan-mediated interactions illustrate
372 how glycan conformation can play a functional role through involvement with agonist
373 binding and LBD conformational dynamics. However, since glycan-mediated
374 interactions are so infrequent, the potentiating effect of glycan-D2 interactions
375 dominates functionally.
376 We quantified the dependence of glycan conformation on agonist binding and
377 LBD conformation by comparing glycan PMFs for different LBD conformations. For
378 GluN2A, we found that glycan-D2 interactions occur more readily when the LBD is
379 closed (calculated using a 1-dimensional projection of our LBD order parameter ξ_{12}, see
380 Methods). This effect was more dramatic for N443-Man5 than for N444-Man5 **(Fig.**
381 **S7A,B)**. A similar relationship was determined for the N491-Man5 glycan of GluN1 **(Fig.**
382 **S7C)**; this is consistent with previous simulations [29] that suggest that N491-Man5 acts
383 as a latch that stabilizes LBD closure. No significant relationship between glycan-D2
384 distance and the presence of an agonist (D-serine, glutamate, or both) in the binding
385 site was observed.
386
387 **DISCUSSION**

388 Here, we characterized the guided-diffusion mechanism that drives D-serine
389 binding to NMDAR LBDs. Instead of binding solely to the GluN1 LBD, we observed
390 substantial D-serine binding to the GluN2A LBD, a subunit widely accepted to bind to
391 the neurotransmitter glutamate. We showed by electrophysiology that D-serine at high
392 concentration can compete against glutamate at GluN2A, which in turn inhibits the
393 channel activity. In the context of synaptic transmission, our finding implies that D-serine
394 could play a role in modulating the strength of synaptic transmission. The synaptic
395 concentration of glutamate ranges from nanomolar concentrations [30] to >1 mM
396 following an action potential [31]. The synaptic concentration of D-serine is unclear,
397 however; the extracellular concentration of D-serine ranges from 5 to 7 μM [32] [33].
398 Possible routes for D-serine to enter the synapse include vesicular release by astroglia
399 [34] and transport by Asc-1 [35].
400 Free energy landscapes computed for GluN2A bound to glutamate [16], D-
401 serine, and glycine all indicate stabilization of the closed LBD bi-lobe, which is the
402 conformational state required for receptor activation. Agonists that can interact
403 extensively with bottom-lobe residues stabilize this state. Since glutamate does this to
404 the greatest extent, it is likely that D-serine does not generate sufficient force to fully
405 gate the ion channel. Subtle differences in the thermodynamics of agonist stabilization
406 suggest that kinetics further distinguish individual agonists. While glutamate has a
407 slightly higher association rate than D-serine, differences between association rates
408 across agonists and subunits is not drastic. We hypothesize that, in order for agonist
409 binding to result in NMDAR activation, the agonist must remain in the binding site long

410 enough to induce closure – we found that this is largely dependent upon the number
411 and strength of stable contacts the agonist forms with both D1 and D2 lobe residues.
412 We determined the role of N-linked glycans in agonist binding and stabilization.
413 Glycans impact agonist binding kinetics less by direct glycan-agonist interactions and
414 more by stabilizing the closed LBD through glycan-D2 interactions. This bias toward
415 LBD closure would increase the agonist residence time and potentiate NMDAR activity.
416 Our adaptation of pathway similarity analysis allowed us to identify clusters of
417 residues critical for binding agonists. This also allowed us to determine that the
418 presence of pathways depends on the degree of LBD closure. We also observed that D-
419 serine binds to GluN2A using similar pathways and residues as glutamate, while the
420 locations of key D-serine cluster residues for GluN1 are different. Applied more broadly
421 to drug-binding simulations, this method of analyzing binding pathways provides a
422 useful framework for gleaning biological insight from noisy and diffusive binding data.
423

424 **METHODS**

425 ***Equilibrium Molecular Dynamics Simulations***

426 A construct of the GluN1/GluN2A dimer based on crystal structure (PDB ID:
427 2A5T [36]) used in our previous study [18] was used as a starting model. The residue
428 numberings are based on the Uniprot numbering for GRIN1 and GRIN2a entries.
429 $Man_5GlcNAc_2$ (Man5) glycans were added using CHARMM-GUI *Glycan Reader &*
430 *Modeler* [37] [38] [39] [40] to asparagine residues 440, 471, 491, and 771 of GluN1 and
431 asparagine residues 443 and 444 of GluN2A in accordance with physiologically relevant
432 glycosylation sites [20]. GluN2A was chosen as the GluN2 subtype both to facilitate

433 comparison with previous simulation studies and because recent evidence has
434 suggested that the GluN2A subtype is the primary subtype at synapses, where D-serine
435 is the dominant co-agonist [4].

436 All systems were solvated in a 140 Å × 110 Å × 110 Å orthorhombic water box
437 with ~150 mM NaCl using CHARMM [41]. All systems were electrically neutral. All
438 simulations in this work were performed using the CHARMM36 forcefield [42] and
439 TIP3P water model [43]. The systems were pre-equilibrated using NAMD 2.13 [44] first
440 using NVT conditions and gradually relaxing backbone-sidechain restraints and then for
441 15 ns using NPT conditions at a pressure of 1 atm and a temperature of 310 K. The pre-
442 equilibrated systems were then simulated on Anton 2 provided by the Pittsburgh
443 Supercomputer Center [45]. A weak center-of-mass restraint of 0.5 kcal mol^{-1} $Å^{-1}$ was
444 applied to GluN2A N, CA, and C atoms of residues 461-463. 507-509, and 523-525 to
445 prevent large protein translational motion. Simulations on Anton 2 were carried out at
446 310 K with the NPT ensemble and with the weak center-of-mass restraint of 0.3 kcal
447 mol^{-1} $Å^{-1}$ in accordance with previous simulations [19]. Additional simulation details are
448 provided in **Dataset S1**.

449

450 ***Identification of binding pathways***

451 Identifying frames in which the ligand is bound in the receptor's binding pocket
452 provides key information about the ligand's binding affinity and the bound ensemble;
453 however, it fails to account for the process by which the ligand enters and leaves the
454 binding pocket. In guided diffusion, the residues that guide the ligand into the binding
455 pocket are critical for promoting the bound state. While imposing a simple distance

456 cutoff is sufficient for identifying the fully bound state, identifying the pathways by which
457 the ligand binds is less trivial. Here, we introduce a “binding chains” paradigm for
458 defining the ligand’s path along the protein. These binding chains are defined from
459 ligand association to dissociation. An association begins when any polar ligand heavy
460 atom comes within 6 Å of any protein polar heavy atom. The ligand is considered
461 associated until is diffuses beyond 10 Å from the protein. The resulting chains are then
462 filtered by contact with the selected “docking” residue(s). Here, we use the conserved
463 arginine residue for each subunit (Arg-523 for GluN1 and Arg-518 for GluN2A) as the
464 essential docking residue. These chains are filtered then split into their “binding” and
465 “unbinding” components by a more specific docking criterion. In our case, we require
466 that the NH1 and NH2 atoms of the conserved arginine be within 4 Å of the ligand
467 carboxyl in accordance with the following scheme:
468
469 Condition 1: Arg NH1 is within 4 Å of the ligand OT1 <u>AND</u> Arg NH2 is within 4 Å of the
470 ligand OT2
471 <u>OR</u>
472 Condition 2: Arg NH2 is within 4 Å of the ligand OT1 <u>AND</u> Arg NH1 is within 4 Å of the
473 ligand OT2
474
475 This scheme accounts for both the crystallographic binding pose (Condition 2) and a
476 “flipped” ligand orientation (Condition 1). Chains that fail to meet these criteria are
477 discarded. Since binding and unbinding pathways can be considered reversible, we
478 combine them in our analysis, reversing the order of the unbinding pathways so that all

pathways have the same directionality. This results in a series of binding pathways we can characterize both geometrically and in terms of key residue interactions.

Pathway Similarity Analysis and Clustering

Pathway Similarity Analysis (PSA) was applied to each binding pathway by monitoring the agonist position as it binds. PSA involves computing a pairwise distance metric between paths that serves as a measure of geometric similarity [21]. The weighted average Hausdorff distance was selected as the path metric because it gave the most geospatially distinct clusters of agonist density around the protein. This weighted average Hausdorff distance was computed for all pairs of paths using the following formula as described in previous work [21] and implemented in the MDAnalysis python package [46][47]. The weighted-average Hausdorff distance between two paths A and B can be expressed as:

$$\delta_H^{w_{\text{avg}}}(A,B) = \frac{1}{2}\left[\frac{1}{|A|}\delta_H^{\text{sum}}(A|B) + \frac{1}{|B|}\delta_H^{\text{sum}}(B|A)\right],$$

where $|A|$ and $|B|$ are the number of frames in paths A and B, respectively, and δ_H^{sum} is the one-sided summed Hausdorff distance from path A to path B,

$$\delta_H^{\text{sum}}(A|B) = \sum_{a\in A} \min_{b\in B} d(a,b) \ .$$

Here, $d(a,b)$ represents the distance between point a of path A and point b in path B. For our system, each point a is the agonist C_α position for a single frame in path A, and

each point b is the agonist C_α position for a single frame in path B. Therefore, $d(a, b)$ represents the Euclidean distance between the agonist C_α's of points in paths A and B. $\delta_H^{\text{sum}}(A|B)$ is then computed by summing the shortest distance from each point a in path A to any point b of path B over all points in path A. Each of the normalized one-sided sums $\delta_H^{\text{sum}}(A|B)$ and $\delta_H^{\text{sum}}(B|A)$ are then averaged with equal weights. This does not give more weight to pathways with more frames, thus removing the temporal component from the analysis. Temporal patterns in binding pathways are analyzed for the spatial clusters separately.

These path pairs were then clustered using hierarchical clustering according to their weighted-average Hausdorff distances with the Ward (minimum variance) linkage criterion as described in previous work [21] and implemented in SciPy [48]. The complete linkage criterion also gave reasonable clustering. This agglomerative metric assigns clusters by successively combining clusters that minimize the sum of squared errors between them. Hierarchical clustering presents an advantage here because it does not assume the number of clusters *a priori*. Rather, final clusters were selected using the Ward distances showed in the dendrograms (see supplemental) as a guide and by overlaying the ligand occupancy density on the protein to ensure that each cluster represents a distinct spatial region of the protein.

Quantifying residue similarity with the overlap coefficient (Szymkiewicz–Simpson coefficient)

To quantify the similarity between two sets of residues A and B, the overlap coefficient was computed by dividing the number of overlapping residues between A

525 and B by the size of the smaller set of residues and is illustrated in the equation below
526 [22]:
527
528 $$OC(A,B) = \frac{|A \cap B|}{\min(|A|,|B|)}.$$
529
530 Scaling the size of the intersection by the smallest set size normalizes the overlap and
531 accounts for the large range in pathway lengths. If A is a subset of B, then $OC(A,B) = 1$.
532 This scaling method is appropriate, since these pathways are stochastic and involve a
533 mixture of random residue contacts and "guiding" residue contacts critical for binding.
534 This would be problematic for the more common Jaccard similarity metric, which scales
535 the intersection by the total size of both sets, where many random contacts increase
536 pathway length and dilute the value of the similarity metric.
537 The overlap coefficient was used to quantify the residue overlap between pairs of
538 pathways in each cluster to validate the spatial clustering and determine whether
539 pathways within clusters involve similar residue contacts. In addition, this metric was
540 used to quantify the similarity between residues involved in D-serine and glutamate
541 binding.
542
543 ***Umbrella Sampling***
544 All-atom models were constructed from monomeric GluN1 (PDB ID: 1PB8 [17])
545 and GluN2A (based on PDB ID: 2A5S [36]). Since no crystal structure of D-serine
546 bound GluN2A exists, LBDs were constructed using MODELLER [49] to fill in missing
547 residues, and sidechain remodeling was performed on those residues using SCWRL4

548 [50]. D-serine and glycine were modelled into the GluN2A LBD by superimposing the
549 conserved arginine of the 2A5S glutamate-bound crystal structure (Arg-518) with the
550 conserved arginine of the D-serine (1PB8) or glycine (1PB7) bound crystal structure,
551 since there exists no crystal structure of GluN2A bound to these agonists. Bound
552 crystallographic waters in the GluN2A (2A5S) and GluN1 (1PB8) structures were
553 retained in the simulations.

554 To generate windows for umbrella sampling, targeted molecular dynamics
555 simulations were performed by "opening" the closed LBD along the order parameter
556 (ξ_1, ξ_2) [16]. Specifically, ξ_1 and ξ_2 are defined as the center of mass distance between
557 the backbone atoms of the following residue selections: ξ_1 is defined by residues 484-
558 485 and 688-689 for GluN1 and residues 485-486 and 689-690 for GluN2A. ξ_2 is
559 defined by residues 405-407 and 714-715 for GluN1 and 413-414 and 713-714 for
560 GluN2A. 205 simulation windows were selected at 1 Å × 1 Å increments. Each window
561 was solvated with a solvent box with dimensions 94 Å × 72 Å × 68 Å and 150 mM
562 NaCl.

563 Umbrella sampling simulations were performed by applying a bias of 2 kcal mol^{-1}
564 to the (ξ_1, ξ_2) order parameter to each of the 205 simulation windows. Equilibration was
565 performed in an NVT ensemble by gradually relaxing backbone and sidechain
566 restraints, and production simulations were carried out in an NPT ensemble at 300 K
567 and 1 atm for best comparison with previously computed NMDAR LBD monomers [16].
568 To ensure that the agonist does not diffuse out of the binding site, a restraint of 2 kcal
569 mol^{-1} $Å^{-1}$ between the carboxyl group of the agonist and the guanidinium group of the
570 conserved arginine (Arg-523 for GluN1 and Arg-518 for GluN2A) was applied if the

571 distance between these groups exceeded 3.2 Å. Previous work has indicated that these
572 restraints do not affect the results but ensures that only the bound population is
573 sampled [16]. A weak center-of-mass restraint of 0.5 kcal mol^{-1} $Å^{-1}$ was used applied to
574 the N, CA, and C atoms of residues 461-463, 507-509, and 523-525 for GluN2A and
575 residues 460-462, 512-514, and 528-530 for GluN1 to prevent translational protein
576 motion. Biased trajectories were mathematically unbiased using the weighted histogram
577 analysis method (WHAM) [51] [52]. 5 ns of production sampling for each window were
578 used to compute the potential of mean force (PMF) for each simulation agonist.
579 Standard deviations of all PMFs were computed by block averaging with ten blocks of
580 trajectory for each window [53].
581
582 ***Computing energetics of glycan conformational dynamics***
583 To quantify glycan conformational dynamics, a glycan-D2 order parameter was
584 defined as the minimum distance between the heavy atoms of the glycans near the
585 binding cleft (N491-Man5 for GluN1 and N443-Man5 and N444-Man5 for GluN2A) and
586 the bottom lobe C_α atoms (residues 537-544 and 663-754 for GluN1 and residues 533-
587 539 and 661-757 for GluN2A). One relative PMF was computed for each of the three
588 near-pocket glycans using a window size of 0.2 Å using all glycosylated datasets. Error
589 for each PMF was quantified using the standard deviation computed by block averaging
590 with five blocks **(Fig. S5A-D)**. Blocks for which the window is not sampled were omitted
591 from the error calculation; this was only necessary for high glycan distances >20 Å. A
592 1D projection of the (ξ_1, ξ_2) order parameter, ξ_{12}, which averages ξ_1 and ξ_2, was used as
593 a single measure of LBD closure for computing glycan PMFs [16][54][55].

594

595 **Electrophysiology**

596 cRNA encoding GluN1-4b and GluN2A was injected into defolliculated *Xenopus*
597 *laevis* oocytes (0.2–0.5 ng total cRNA per oocyte). The oocytes were incubated in
598 recovery medium (50% L-15 medium (Hyclone) buffered by 15mM Na-HEPES at a final
599 pH of 7.4), supplemented with 100 μg mL^{-1} streptomycin, and 100 U mL^{-1} penicillin at
600 18°C. Two electrode voltage clamp (TEVC; Axoclamp-2B) recording was performed
601 between 24 to 48 hours after injection using an extracellular solution containing 5 mM
602 HEPES, 100 mM NaCl, 0.3 mM $BaCl_2$, 10mM Tricine at final pH 7.4 (adjusted with
603 KOH). The current was measured using agarose-tipped microelectrode (0.4–0.9 MΩ) at
604 the holding potential of −60 mV. Maximal response currents were evoked by 50 μM of
605 D-serine and 100 μM of L-glutamate. Data was acquired by the program PatchMaster
606 (HEKA) and analyzed by Origin 8 (OriginLab Corp).

607

608 **Acknowledgements**

609 Anton 2 computer time (MCB130045P) was provided by the Pittsburgh Supercomputing
610 Center (PSC) through NIH grant R01GM116961 (to A.Y.L.); the Anton 2 machine at
611 PSC was generously made available by D.E. Shaw Research. We also used resources
612 provided by the Maryland Advanced Research Computing Center (MARCC) at Johns
613 Hopkins University. This work was funded by the Johns Hopkins Catalyst Award (to
614 A.Y.L.); NIH T32GM135131 (to R.A.Y. and S.J.B.); NIH NS111745 and MH085926 (to
615 H.F.); Robertson funds at CSHL, Doug Fox Alzheimer's fund, Austin's purpose,
616 Heartfelt Wing Alzheimer's fund, and the Gertrude and Louis Feil Family Trust (to H.F.).

617

618 **Author Contributions**

619 R.A.Y. conducted molecular dynamics simulations; R.A.Y., S.J.B., and A.Y.L. analyzed
620 the results; T.-H.C. and H.F. designed and conducted experiments related to
621 electrophysiology; R.A.Y., T.-H.C., H.F., and A.Y.L. wrote the manuscript.

622

623 **Competing Interests**

624 The authors declare no competing interests.

625

626 **References**

627 (1) Johnson, J. W.; Ascher, P. Glycine Potentiates the NMDA Response in Cultured
628 Mouse Brain Neurons. *Nature* **1987**, *325* (6104), 529–531.
629 https://doi.org/10.1038/325529a0.

630 (2) Forsythe, I. D.; Westbrook, G. L.; Mayer, M. L. Modulation of Excitatory Synaptic
631 Transmission by Glycine and Zinc in Cultures of Mouse Hippocampal Neurons. *J.*
632 *Neurosci.* **1988**, *8* (10), 3733–3741. https://doi.org/10.1523/jneurosci.08-10-
633 03733.

634 (3) Kleckner, N. W.; Dingledine, R. Requirement for Glycine in Activation of NMDA
635 Receptors Expressed in Xenopus Oocytes. *Science (80-.).* **1988**, *241* (4867),
636 835–837. https://doi.org/10.1126/science.2841759.

637 (4) Papouin, T.; Ladépêche, L.; Ruel, J.; Sacchi, S.; Labasque, M.; Hanini, M.; Groc,
638 L.; Pollegioni, L.; Mothet, J. P.; Oliet, S. H. R. Synaptic and Extrasynaptic NMDA
639 Receptors Are Gated by Different Endogenous Coagonists. *Cell* **2012**, *150* (3),

640 633–646. https://doi.org/10.1016/j.cell.2012.06.029.
641 (5) Wolosker, H.; Blackshaw, S.; Snyder, S. H. Serine Racemase: A Glial Enzyme
642 Synthesizing D-Serine to Regulate Glutamate-N-Methyl-D-Aspartate
643 Neurotransmission. *Proc. Natl. Acad. Sci. U. S. A.* **1999**, *96* (23), 13409–13414.
644 https://doi.org/10.1073/pnas.96.23.13409.
645 (6) Miya, K.; Inoue, R.; Takata, Y.; Abe, M.; Natsume, R.; Sakimura, K.; Hongou, K.;
646 Miyawaki, T.; Mori, H. Serine Racemase Is Predominantly Localized in Neurons in
647 Mouse Brain. *J. Comp. Neurol.* **2008**, *510* (6), 641–654.
648 https://doi.org/10.1002/cne.21822.
649 (7) Balu, D. T.; Takagi, S.; Puhl, M. D.; Benneyworth, M. A.; Coyle, J. T. D-Serine
650 and Serine Racemase Are Localized to Neurons in the Adult Mouse and Human
651 Forebrain. *Cell. Mol. Neurobiol.* **2014**, *34* (3), 419–435.
652 https://doi.org/10.1007/s10571-014-0027-z.
653 (8) Rutter, A. R.; Fradley, R. L.; Garrett, E. M.; Chapman, K. L.; Lawrence, J. M.;
654 Rosahl, T. W.; Patel, S. Evidence from Gene Knockout Studies Implicates Asc-1
655 as the Primary Transporter Mediating D-Serine Reuptake in the Mouse CNS. *Eur.*
656 *J. Neurosci.* **2007**, *25* (6), 1757–1766. https://doi.org/10.1111/j.1460-
657 9568.2007.05446.x.
658 (9) Coyle, J. T.; Balu, D.; Wolosker, H. D-Serine, the Shape-Shifting NMDA Receptor
659 Co-Agonist. *Neurochem. Res.* **2020**, 1–10. https://doi.org/10.1007/s11064-020-
660 03014-1.
661 (10) Henneberger, C.; Papouin, T.; Oliet, S. H. R.; Rusakov, D. A. Long-Term
662 Potentiation Depends on Release of d-Serine from Astrocytes. *Nature* **2010**, *463*

663 (7278), 232–236. https://doi.org/10.1038/nature08673.
664 (11) Peyrovian, B.; Rosenblat, J. D.; Pan, Z.; Iacobucci, M.; Brietzke, E.; McIntyre, R.
665 S. The Glycine Site of NMDA Receptors: A Target for Cognitive Enhancement in
666 Psychiatric Disorders. *Progress in Neuro-Psychopharmacology and Biological*
667 *Psychiatry*. Elsevier Inc. June 8, 2019, pp 387–404.
668 https://doi.org/10.1016/j.pnpbp.2019.02.001.
669 (12) MacKay, M. A. B.; Kravtsenyuk, M.; Thomas, R.; Mitchell, N. D.; Dursun, S. M.;
670 Baker, G. B. D-Serine: Potential Therapeutic Agent and/or Biomarker in
671 Schizophrenia and Depression? *Front. Psychiatry* **2019**, *10* (FEB), 18–23.
672 https://doi.org/10.3389/fpsyt.2019.00025.
673 (13) Kantrowitz, J. T.; Malhotra, A. K.; Cornblatt, B.; Silipo, G.; Balla, A.; Suckow, R.
674 F.; D'Souza, C.; Saksa, J.; Woods, S. W.; Javitt, D. C. High Dose D-Serine in the
675 Treatment of Schizophrenia. *Schizophr. Res.* **2010**, *121* (1–3), 125–130.
676 https://doi.org/10.1016/j.schres.2010.05.012.
677 (14) Heresco-Levy, U.; Javitt, D. C.; Ebstein, R.; Vass, A.; Lichtenberg, P.; Bar, G.;
678 Catinari, S.; Ermilov, M. D-Serine Efficacy as Add-on Pharmacotherapy to
679 Risperidone and Olanzapine for Treatment-Refractory Schizophrenia. *Biol.*
680 *Psychiatry* **2005**, *57* (6), 577–585. https://doi.org/10.1016/j.biopsych.2004.12.037.
681 (15) Mayer, M. L. The Challenge of Interpreting Glutamate-Receptor Ion-Channel
682 Structures. *Biophysical Journal*. Biophysical Society November 21, 2017, pp
683 2143–2151. https://doi.org/10.1016/j.bpj.2017.07.028.
684 (16) Yao, Y.; Belcher, J.; Berger, A. J.; Mayer, M. L.; Lau, A. Y. Conformational
685 Analysis of NMDA Receptor GluN1, GluN2, and GluN3 Ligand-Binding Domains

686 Reveals Subtype-Specific Characteristics. *Structure* **2013**, *21* (10), 1788–1799.
687 https://doi.org/10.1016/j.str.2013.07.011.
688 (17) Furukawa, H.; Gouaux, E. Mechanisms of Activation, Inhibition and Specificity:
689 Crystal Structures of the NMDA Receptor NR1 Ligand-Binding Core. *EMBO J.*
690 **2003**, *22* (12), 2873–2885. https://doi.org/10.1093/emboj/cdg303.
691 (18) Yu, A.; Lau, A. Y. Glutamate and Glycine Binding to the NMDA Receptor.
692 *Structure* **2018**, *26* (7), 1035-1043.e2. https://doi.org/10.1016/j.str.2018.05.004.
693 (19) Yu, A.; Salazar, H.; Plested, A. J. R.; Lau, A. Y. Neurotransmitter Funneling
694 Optimizes Glutamate Receptor Kinetics. *Neuron* **2018**, *97* (1), 139-149.e4.
695 https://doi.org/10.1016/j.neuron.2017.11.024.
696 (20) Kaniakova, M.; Lichnerova, K.; Skrenkova, K.; Vyklicky, L.; Horak, M. Biochemical
697 and Electrophysiological Characterization of *N*- Glycans on NMDA Receptor
698 Subunits. *J. Neurochem.* **2016**, *138* (4), 546–556.
699 https://doi.org/10.1111/jnc.13679.
700 (21) Seyler, S. L.; Kumar, A.; Thorpe, M. F.; Beckstein, O. Path Similarity Analysis: A
701 Method for Quantifying Macromolecular Pathways. *PLoS Comput. Biol.* **2015**, *11*
702 (10), 1004568. https://doi.org/10.1371/journal.pcbi.1004568.
703 (22) Vijaymeena, M. K.; Kavitha, K. A SURVEY ON SIMILARITY MEASURES IN
704 TEXT MINING. *Mach. Learn. Appl. An Int. J.* **2016**, *3* (1).
705 https://doi.org/10.5121/mlaij.2016.3103.
706 (23) Jalali-Yazdi, F.; Chowdhury, S.; Yoshioka, C.; Gouaux, E. Mechanisms for Zinc
707 and Proton Inhibition of the GluN1/GluN2A NMDA Receptor. *Cell* **2018**, *175* (6),
708 1520-1532.e15. https://doi.org/10.1016/j.cell.2018.10.043.

709 (24) Sinitskiy, A. V.; Stanley, N. H.; Hackos, D. H.; Hanson, J. E.; Sellers, B. D.;
710 Pande, V. S. Computationally Discovered Potentiating Role of Glycans on NMDA
711 Receptors. *Sci. Rep.* **2017**, *7* (1), 1–10. https://doi.org/10.1038/srep44578.
712 (25) Dolino, D. M.; Adariani, S. R.; Shaikh, S. A.; Jayaraman, V.; Sanabria, H.
713 Conformational Selection and Submillisecond Dynamics of the Ligand-Binding
714 Domain of the N-Methyl-d-Aspartate Receptor. *J. Biol. Chem.* **2016**, *291* (31),
715 16175. https://doi.org/10.1074/JBC.M116.721274.
716 (26) Rajab, S.; Bismin, L.; Schwarze, S.; Pinggera, A.; Greger, I. H.; Neuweiler, H.
717 Allosteric Coupling of Sub-Millisecond Clamshell Motions in Ionotropic Glutamate
718 Receptor Ligand-Binding Domains. *Commun. Biol. 2021 41* **2021**, *4* (1), 1–11.
719 https://doi.org/10.1038/s42003-021-02605-0.
720 (27) Snyder, S. H.; Mustafa, A. K.; Kim, P. M. D-Serine as a Putative Glial
721 Neurotransmitter. *Neuron Glia Biol.* **2004**, *1* (3), 275–281.
722 https://doi.org/10.1017/S1740925X05000141.
723 (28) Dror, R. O.; Pan, A. C.; Arlow, D. H.; Borhani, D. W.; Maragakis, P.; Shan, Y.; Xu,
724 H.; Shaw, D. E. Pathway and Mechanism of Drug Binding to G-Protein-Coupled
725 Receptors. *Proc. Natl. Acad. Sci. U. S. A.* **2011**, *108* (32), 13118–13123.
726 https://doi.org/10.1073/pnas.1104614108.
727 (29) Sinitskiy, A. V.; Pande, V. S. Simulated Dynamics of Glycans on Ligand-Binding
728 Domain of NMDA Receptors Reveals Strong Dynamic Coupling between Glycans
729 and Protein Core. *J. Chem. Theory Comput.* **2017**, *13* (11), 5496–5505.
730 https://doi.org/10.1021/acs.jctc.7b00817.
731 (30) Chiu, D. N.; Jahr, C. E. Extracellular Glutamate in the Nucleus Accumbens Is

732 Nanomolar in Both Synaptic and Non-Synaptic Compartments. *Cell Rep.* **2017**, *18*
733 (11), 2576–2583. https://doi.org/10.1016/j.celrep.2017.02.047.
734 (31) Dzubay, J. A.; Jahr, C. E. The Concentration of Synaptically Released Glutamate
735 Outside of the Climbing Fiber-Purkinje Cell Synaptic Cleft. *J. Neurosci.* **1999**, *19*
736 (13), 5265–5274. https://doi.org/10.1523/jneurosci.19-13-05265.
737 (32) Matsui, T. -a; Sekiguchi, M.; Hashimoto, A.; Tomita, U.; Nishikawa, T.; Wada, K.
738 Functional Comparison of D-Serine and Glycine in Rodents: The Effect on Cloned
739 NMDA Receptors and the Extracellular Concentration. *J. Neurochem.* **1995**, *65*
740 (1), 454–458. https://doi.org/10.1046/j.1471-4159.1995.65010454.x.
741 (33) Hashimoto, A.; Oka, T.; Nishikawa, T. Extracellular Concentration of Endogenous
742 Free D-Serine in the Rat Brain as Revealed by in Vivo Microdialysis.
743 *Neuroscience* **1995**, *66* (3), 635–643. https://doi.org/10.1016/0306-
744 4522(94)00597-X.
745 (34) Mothet, J. P.; Pollegioni, L.; Ouanounou, G.; Martineau, M.; Fossier, P.; Baux, G.
746 Glutamate Receptor Activation Triggers a Calcium-Dependent and SNARE
747 Protein-Dependent Release of the Gliotransmitter D-Serine. *Proc. Natl. Acad. Sci.*
748 *U. S. A.* **2005**, *102* (15), 5606–5611. https://doi.org/10.1073/pnas.0408483102.
749 (35) Sason, H.; Billard, J. M.; Smith, G. P.; Safory, H.; Neame, S.; Kaplan, E.;
750 Rosenberg, D.; Zubedat, S.; Foltyn, V. N.; Christoffersen, C. T.; Bundgaard, C.;
751 Thomsen, C.; Avital, A.; Christensen, K. V.; Wolosker, H. Asc-1 Transporter
752 Regulation of Synaptic Activity via the Tonic Release of -Serine in the Forebrain.
753 *Cereb. Cortex* **2017**, *27* (2), 1573–1587. https://doi.org/10.1093/cercor/bhv350.
754 (36) Furukawa, H.; Singh, S. K.; Mancusso, R.; Gouaux, E. Subunit Arrangement and

755 Function in NMDA Receptors. *Nature* **2005**, *438* (7065), 185–192.
756 https://doi.org/10.1038/nature04089.
757 (37) Jo, S.; Kim, T.; Iyer, V. G.; Im, W. CHARMM-GUI: A Web-Based Graphical User
758 Interface for CHARMM. *J. Comput. Chem.* **2008**, *29* (11), 1859–1865.
759 https://doi.org/10.1002/jcc.20945.
760 (38) Jo, S.; Song, K. C.; Desaire, H.; MacKerell, A. D.; Im, W. Glycan Reader:
761 Automated Sugar Identification and Simulation Preparation for Carbohydrates and
762 Glycoproteins. *J. Comput. Chem.* **2011**, *32* (14), 3135–3141.
763 https://doi.org/10.1002/jcc.21886.
764 (39) Park, S. J.; Lee, J.; Patel, D. S.; Ma, H.; Lee, H. S.; Jo, S.; Im, W. Glycan Reader
765 Is Improved to Recognize Most Sugar Types and Chemical Modifications in the
766 Protein Data Bank. *Bioinformatics* **2017**, *33* (19), 3051–3057.
767 https://doi.org/10.1093/bioinformatics/btx358.
768 (40) Park, S. J.; Lee, J.; Qi, Y.; Kern, N. R.; Lee, H. S.; Jo, S.; Joung, I.; Joo, K.; Lee,
769 J.; Im, W. CHARMM-GUI Glycan Modeler for Modeling and Simulation of
770 Carbohydrates and Glycoconjugates. *Glycobiology* **2019**, *29* (4), 320–331.
771 https://doi.org/10.1093/glycob/cwz003.
772 (41) Brooks, B. R.; Brooks, C. L.; Mackerell, A. D.; Nilsson, L.; Petrella, R. J.; Roux, B.;
773 Won, Y.; Archontis, G.; Bartels, C.; Boresch, S.; Caflisch, A.; Caves, L.; Cui, Q.;
774 Dinner, A. R.; Feig, M.; Fischer, S.; Gao, J.; Hodoscek, M.; Im, W.; Kuczera, K.;
775 Lazaridis, T.; Ma, J.; Ovchinnikov, V.; Paci, E.; Pastor, R. W.; Post, C. B.; Pu, J.
776 Z.; Schaefer, M.; Tidor, B.; Venable, R. M.; Woodcock, H. L.; Wu, X.; Yang, W.;
777 York, D. M.; Karplus, M. CHARMM: The Biomolecular Simulation Program. *J.*

Comput. Chem. **2009**, *30* (10), 1545–1614. https://doi.org/10.1002/jcc.21287.

(42) MacKerell, A. D.; Bashford, D.; Bellott, M.; Dunbrack, R. L.; Evanseck, J. D.; Field, M. J.; Fischer, S.; Gao, J.; Guo, H.; Ha, S.; Joseph-McCarthy, D.; Kuchnir, L.; Kuczera, K.; Lau, F. T. K.; Mattos, C.; Michnick, S.; Ngo, T.; Nguyen, D. T.; Prodhom, B.; Reiher, W. E.; Roux, B.; Schlenkrich, M.; Smith, J. C.; Stote, R.; Straub, J.; Watanabe, M.; Wiórkiewicz-Kuczera, J.; Yin, D.; Karplus, M. All-Atom Empirical Potential for Molecular Modeling and Dynamics Studies of Proteins. *J. Phys. Chem. B* **1998**, *102* (18), 3586–3616. https://doi.org/10.1021/jp973084f.

(43) Jorgensen, W. L.; Chandrasekhar, J.; Madura, J. D.; Impey, R. W.; Klein, M. L. Comparison of Simple Potential Functions for Simulating Liquid Water. *J. Chem. Phys.* **1983**, *79* (2), 926–935. https://doi.org/10.1063/1.445869.

(44) Phillips, J. C.; Braun, R.; Wang, W.; Gumbart, J.; Tajkhorshid, E.; Villa, E.; Chipot, C.; Skeel, R. D.; Kalé, L.; Schulten, K. Scalable Molecular Dynamics with NAMD. *Journal of Computational Chemistry*. John Wiley and Sons Inc. December 1, 2005, pp 1781–1802. https://doi.org/10.1002/jcc.20289.

(45) Shaw, D. E.; Grossman, J. P.; Bank, J. A.; Batson, B.; Butts, J. A.; Chao, J. C.; Deneroff, M. M.; Dror, R. O.; Even, A.; Fenton, C. H.; Forte, A.; Gagliardo, J.; Gill, G.; Greskamp, B.; Ho, C. R.; Ierardi, D. J.; Iserovich, L.; Kuskin, J. S.; Larson, R. H.; Layman, T.; Lee, L. S.; Lerer, A. K.; Li, C.; Killebrew, D.; Mackenzie, K. M.; Mok, S. Y. H.; Moraes, M. A.; Mueller, R.; Nociolo, L. J.; Peticolas, J. L.; Quan, T.; Ramot, D.; Salmon, J. K.; Scarpazza, D. P.; Ben Schafer, U.; Siddique, N.; Snyder, C. W.; Spengler, J.; Tang, P. T. P.; Theobald, M.; Toma, H.; Towles, B.; Vitale, B.; Wang, S. C.; Young, C. Anton 2: Raising the Bar for Performance and

Programmability in a Special-Purpose Molecular Dynamics Supercomputer. In *International Conference for High Performance Computing, Networking, Storage and Analysis, SC*; IEEE Computer Society, 2014; Vol. 2015-January, pp 41–53. https://doi.org/10.1109/SC.2014.9.

(46) Michaud-Agrawal, N.; Denning, E. J.; Woolf, T. B.; Beckstein, O. MDAnalysis: A Toolkit for the Analysis of Molecular Dynamics Simulations. *J. Comput. Chem.* **2011**, *32* (10), 2319–2327. https://doi.org/10.1002/jcc.21787.

(47) Gowers, R.; Linke, M.; Barnoud, J.; Reddy, T.; Melo, M.; Seyler, S.; Domański, J.; Dotson, D.; Buchoux, S.; Kenney, I.; Beckstein, O. MDAnalysis: A Python Package for the Rapid Analysis of Molecular Dynamics Simulations. In *Proceedings of the 15th Python in Science Conference*; SciPy, 2016; pp 98–105. https://doi.org/10.25080/majora-629e541a-00e.

(48) Virtanen, P.; Gommers, R.; Oliphant, T. E.; Haberland, M.; Reddy, T.; Cournapeau, D.; Burovski, E.; Peterson, P.; Weckesser, W.; Bright, J.; van der Walt, S. J.; Brett, M.; Wilson, J.; Millman, K. J.; Mayorov, N.; Nelson, A. R. J.; Jones, E.; Kern, R.; Larson, E.; Carey, C. J.; Polat, İ.; Feng, Y.; Moore, E. W.; VanderPlas, J.; Laxalde, D.; Perktold, J.; Cimrman, R.; Henriksen, I.; Quintero, E. A.; Harris, C. R.; Archibald, A. M.; Ribeiro, A. H.; Pedregosa, F.; van Mulbregt, P.; Vijaykumar, A.; Bardelli, A. Pietro; Rothberg, A.; Hilboll, A.; Kloeckner, A.; Scopatz, A.; Lee, A.; Rokem, A.; Woods, C. N.; Fulton, C.; Masson, C.; Häggström, C.; Fitzgerald, C.; Nicholson, D. A.; Hagen, D. R.; Pasechnik, D. V.; Olivetti, E.; Martin, E.; Wieser, E.; Silva, F.; Lenders, F.; Wilhelm, F.; Young, G.; Price, G. A.; Ingold, G. L.; Allen, G. E.; Lee, G. R.; Audren, H.; Probst, I.; Dietrich,

824 J. P.; Silterra, J.; Webber, J. T.; Slavič, J.; Nothman, J.; Buchner, J.; Kulick, J.;
825 Schönberger, J. L.; de Miranda Cardoso, J. V.; Reimer, J.; Harrington, J.;
826 Rodríguez, J. L. C.; Nunez-Iglesias, J.; Kuczynski, J.; Tritz, K.; Thoma, M.;
827 Newville, M.; Kümmerer, M.; Bolingbroke, M.; Tartre, M.; Pak, M.; Smith, N. J.;
828 Nowaczyk, N.; Shebanov, N.; Pavlyk, O.; Brodtkorb, P. A.; Lee, P.; McGibbon, R.
829 T.; Feldbauer, R.; Lewis, S.; Tygier, S.; Sievert, S.; Vigna, S.; Peterson, S.; More,
830 S.; Pudlik, T.; Oshima, T.; Pingel, T. J.; Robitaille, T. P.; Spura, T.; Jones, T. R.;
831 Cera, T.; Leslie, T.; Zito, T.; Krauss, T.; Upadhyay, U.; Halchenko, Y. O.;
832 Vázquez-Baeza, Y. SciPy 1.0: Fundamental Algorithms for Scientific Computing
833 in Python. *Nat. Methods* **2020**, *17* (3), 261–272. https://doi.org/10.1038/s41592-
834 019-0686-2.
835 (49) Webb, B.; Sali, A. Comparative Protein Structure Modeling Using MODELLER.
836 *Curr. Protoc. Bioinforma.* **2016**, *2016*, 5.6.1-5.6.37. https://doi.org/10.1002/cpbi.3.
837 (50) Krivov, G. G.; Shapovalov, M. V.; Dunbrack, R. L. Improved Prediction of Protein
838 Side-Chain Conformations with SCWRL4. *Proteins Struct. Funct. Bioinforma.*
839 **2009**, *77* (4), 778–795. https://doi.org/10.1002/prot.22488.
840 (51) Kumar, S.; Rosenberg, J. M.; Bouzida, D.; Swendsen, R. H.; Kollman, P. A. THE
841 Weighted Histogram Analysis Method for Free-energy Calculations on
842 Biomolecules. I. The Method. *J. Comput. Chem.* **1992**, *13* (8), 1011–1021.
843 https://doi.org/10.1002/jcc.540130812.
844 (52) Souaille, M.; Roux, B. Extension to the Weighted Histogram Analysis Method:
845 Combining Umbrella Sampling with Free Energy Calculations. *Comput. Phys.*
846 *Commun.* **2001**, *135* (1), 40–57. https://doi.org/10.1016/S0010-4655(00)00215-0.

847 (53) Grossfield, A.; Zuckerman, D. M. Chapter 2 Quantifying Uncertainty and Sampling
848 Quality in Biomolecular Simulations. *Annual Reports in Computational Chemistry*.
849 NIH Public Access 2009, pp 23–48. https://doi.org/10.1016/S1574-
850 1400(09)00502-7.
851 (54) Wied, T. J.; Chin, A. C.; Lau, A. Y. High Conformational Variability in the GluK2
852 Kainate Receptor Ligand-Binding Domain. *Structure* **2019**, *27* (1), 189-195.e2.
853 https://doi.org/10.1016/j.str.2018.09.008.
854 (55) Chin, A. C.; Yovanno, R. A.; Wied, T. J.; Gershman, A.; Lau, A. Y. D-Serine
855 Potently Drives Ligand-Binding Domain Closure in the Ionotropic Glutamate
856 Receptor GluD2. *Structure* **2020**, *28* (10), 1168-1178.e2.
857 https://doi.org/10.1016/j.str.2020.07.005.
858
859

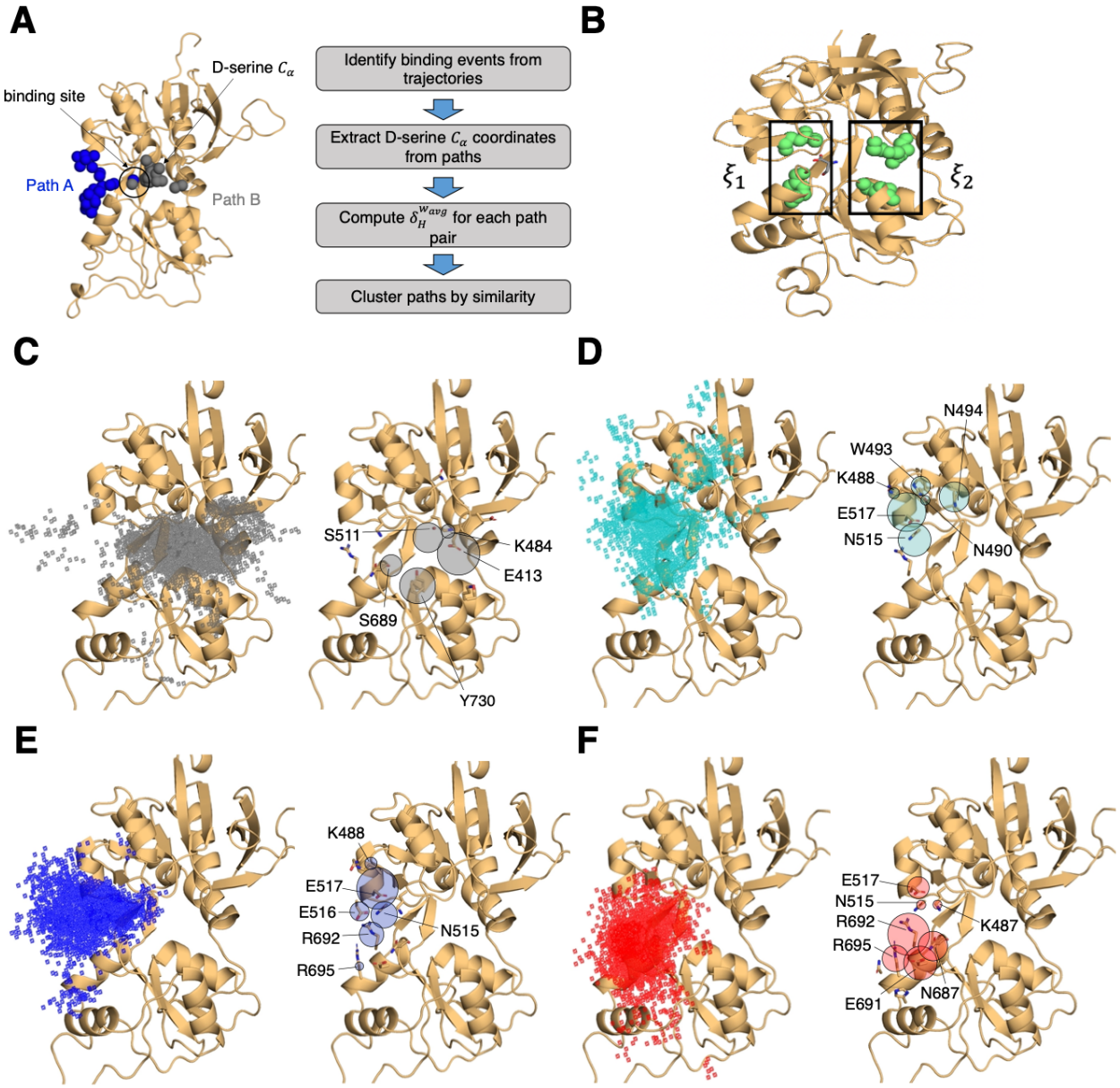

Fig. 1. Identifying D-serine binding pathways for GluN2A using pathway similarity analysis (PSA). **(A)** Overview of the PSA workflow for quantifying similarity between D-serine binding pathways. **(B)** 2-dimensional order parameter (ξ_1, ξ_2) that describes the degree of GluN2A LBD closure. For each of the above **(C-F)**, the left image shows D-serine density, while the right image shows the residues most frequently contacted by D-serine as it enters/leaves the binding site for each cluster. Labeled residues demonstrate ≥ 0.2 fractional occurrence defined relative to the most contacted residue in each cluster, but all residues with ≥ 0.1 fractional occurrence are shown in stick representation (see **Dataset S5**). **(C)** Cluster 1 involves residues of the ξ_2 face of the LBD. **(D)** Cluster 2 involves residues of the ξ_1 face of the D1 lobe. **(E)** In Cluster 3, D-serine zigzags between D1 and D2 lobe residues of the ξ_1 face. **(F)** Cluster 4 primarily involves D2 lobe residues on the ξ_1 face.

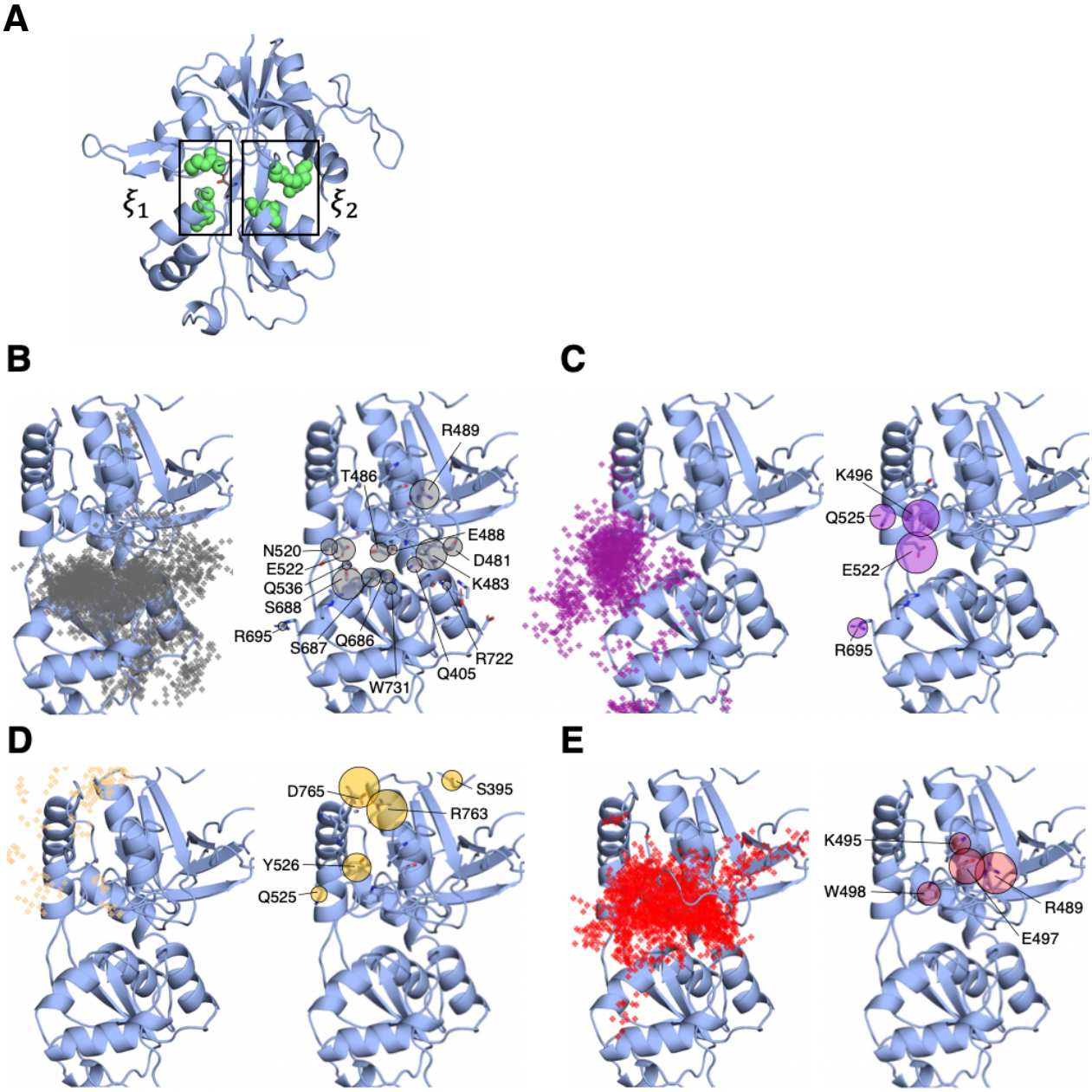

Fig. 2. Identifying D-serine binding pathways for GluN1 using pathway similarity analysis (PSA). **(A)** 2-dimensional order parameter (ξ_1, ξ_2) that describes the degree of GluN1 LBD closure. For each of the above **(B-E)**, the left image shows D-serine density, while the right image shows the residues most frequently contacted by D-serine as it enters/leaves the binding site for each cluster. Labeled residues demonstrate ≥ 0.2 fractional occurrence defined relative to the most contacted residue in each cluster, but all residues with ≥ 0.1 fractional occurrence are shown in stick representation (see **Dataset S6**). **(B)** In Cluster 1, D-Serine contacts residues on the ξ_2 face of the LBD. **(C)** Cluster 2 involves interactions with both D1 and D2 residues of the ξ_1 face. **(D)** Cluster 3 involves contacts with residues at the top of the D1 lobe on the ξ_1 face. **(E)** Cluster 4 is defined by interactions with D1 loop 2 that reaches into solution.

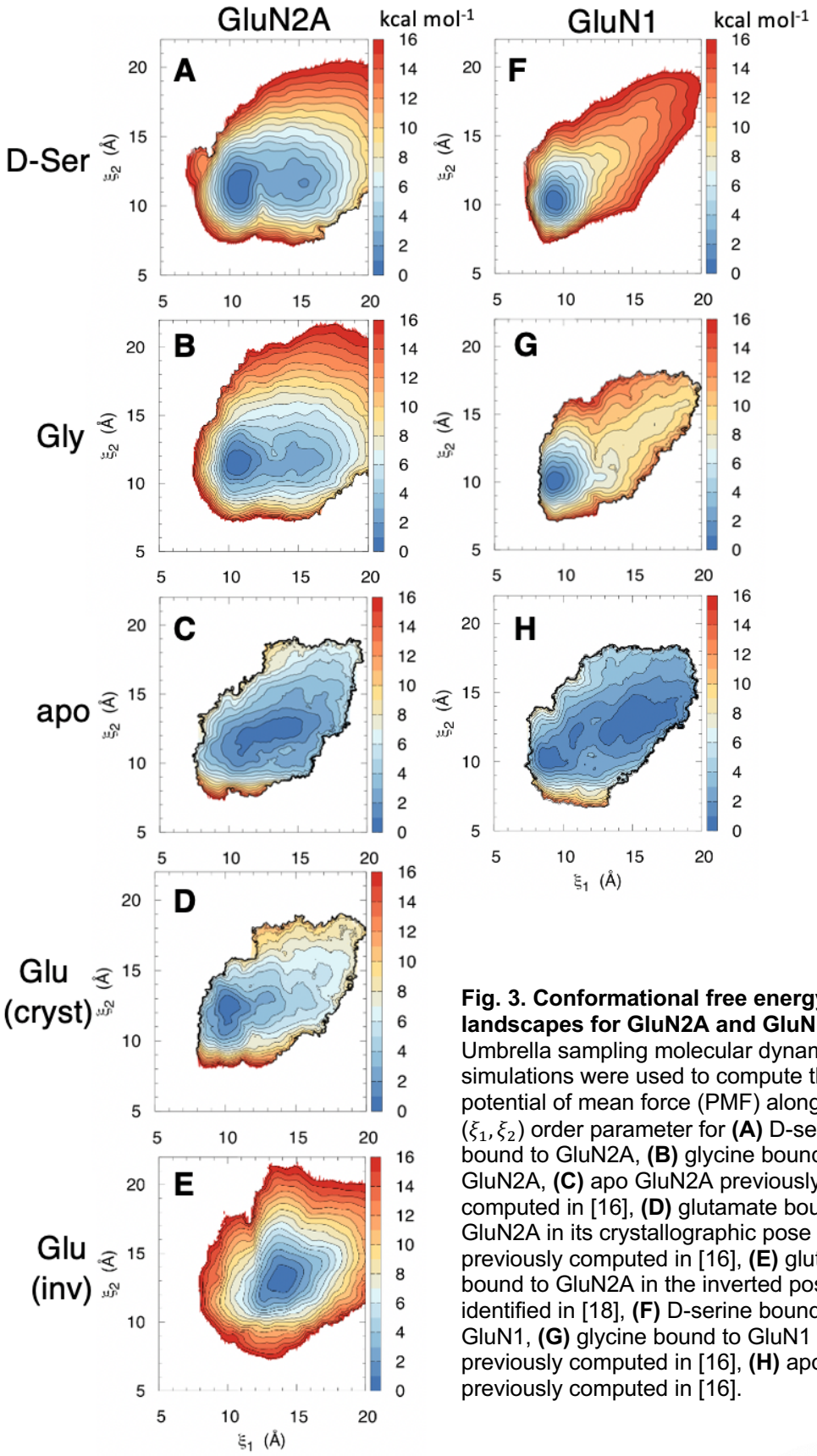

Fig. 3. Conformational free energy landscapes for GluN2A and GluN1 LBDs. Umbrella sampling molecular dynamics simulations were used to compute the potential of mean force (PMF) along the (ξ_1, ξ_2) order parameter for **(A)** D-serine bound to GluN2A, **(B)** glycine bound to GluN2A, **(C)** apo GluN2A previously computed in [16], **(D)** glutamate bound to GluN2A in its crystallographic pose previously computed in [16], **(E)** glutamate bound to GluN2A in the inverted pose identified in [18], **(F)** D-serine bound to GluN1, **(G)** glycine bound to GluN1 previously computed in [16], **(H)** apo GluN1 previously computed in [16].

885

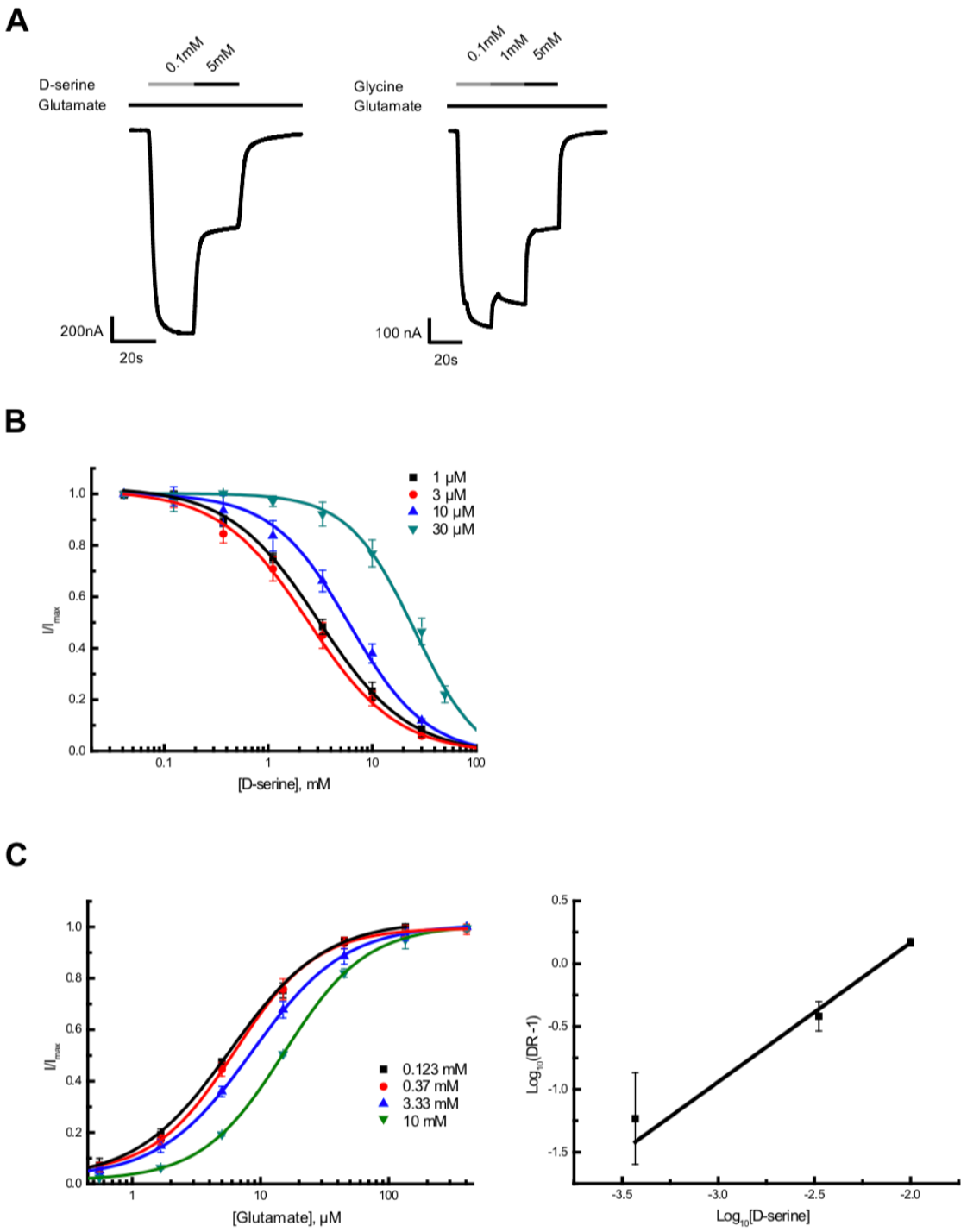

Fig. 4. D-serine completes glutamate binding as an antagonist at high concentration. (A) Representative Two-electrode voltage clamp (TEVC) recording on GluN1/GluN2A NMDARs expressing oocytes. The trace showed GluN1 agonist D-serine inhibited the NMDAR current at a high concentration. 6 μM of glutamate was present throughout the recording. (**B)** Glutamate-concentration dependent dose-response curves of high-concentration D-serine inhibition. (**C)** D-serine-concentration dependent dose-response curves of glutamate potentiation (left). Schild plot analysis of D-serine competition on glutamate (right). The calculated slope of the Schild plot was 1.11±0.13 and the intercept was 2.38±0.26. DR stands for dose ratio. All the dose-response experiments were repeated at least four times.

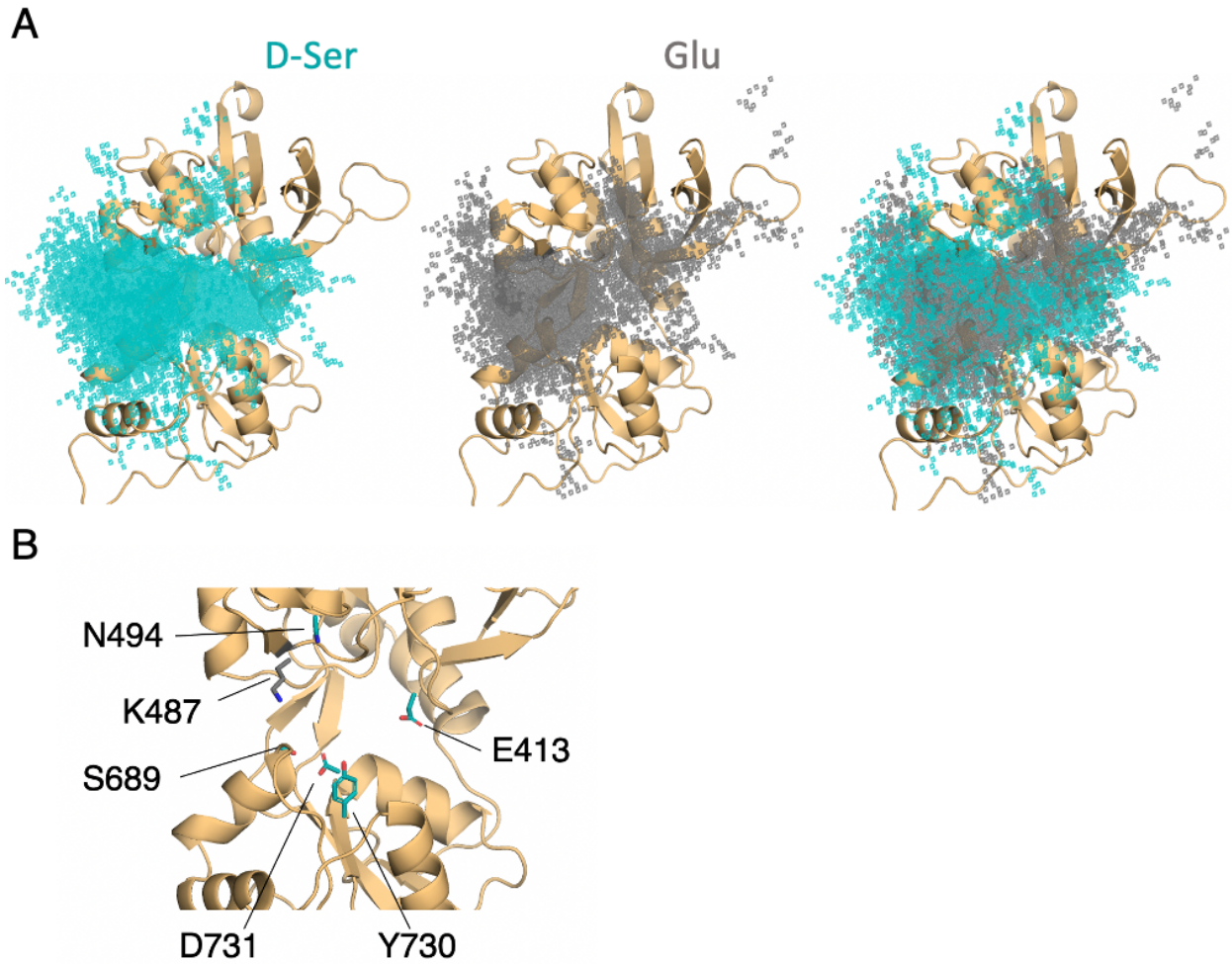

Fig. 5. Comparison of D-serine and glutamate binding to GluN2A. (A) Overlay of D-serine (teal) and glutamate (gray) density. **(B)** Residues that distinguish D-serine (teal) from glutamate (gray) binding pathways (see **Dataset S7**).

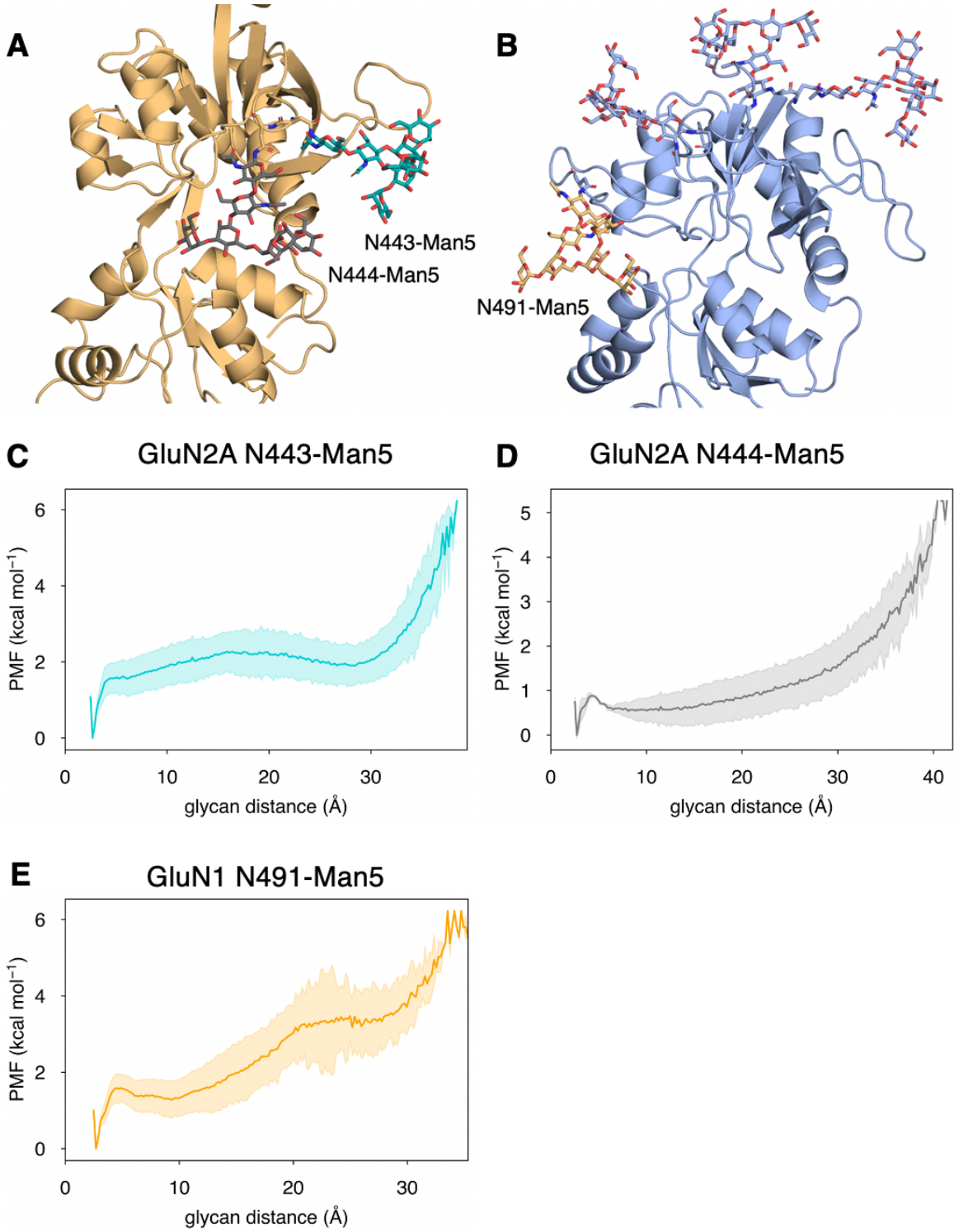

Fig. 6. Conformational dynamics of near-pocket glycans. N-linked $Man_5GlcNAc_2$ (Man5) glycans **(A)** N443-Man5 and N444-Man5 for GluN2A and **(B)** N491-Man5 for GluN1. Glycan conformational energy landscapes for **(C)** GluN2A N443-Man5, **(D)** GluN2A N444-Man5, and **(E)** GluN1 N491-Man5 were obtained by computing the minimum distance between all glycan heavy atoms and D2 lobe residues and binning the distribution from all glycosylated simulation systems. Shaded error regions were computed using a block-averaging scheme described in Methods.